Journal of the European Ceramic Society **18** (1998) 1227–1234

PII: S0955-2219(98)00047-8
0955-2219/98/$—see front matter

Electron Microscopy and Microanalysis of Advanced Materials

Gareth Thomas[a]*† and Mani Gopal[b]

[a]Department of Materials Science and Mineral Engineering, University of California, Berkeley CA 94720, USA
[b]Center for Advanced Materials Lawrence Berkeley National Laboratory Berkeley, CA 94720, USA

Abstract

The characterization of advanced ceramics requires the application of advanced electron microscopy, diffraction and microanalysis. Examples are given here of high resolution (atomic) imaging and microanalysis by energy loss spectroscopy together with their main limitations. These limitations inevitably refer to instrumentation capabilities, and especially the quality and thinness restrictions of specimens. Examples are presented of atomic resolution for structure analysis of nanostructure/fiber ceramics and parallel energy loss spectroscopy and energy filtering for evaluating processing problems in BN–SiC fiber composites. © *1998 Elsevier Science Limited. All rights reserved*

1 Introduction

Materials for advanced applications require superior properties which must be attained by economic and consistent processing routines. In principle, by understanding the processing–structure–properties interactions, which is what materials science is all about, it should be possible to design or tailor materials for such conditions. Since properties depend upon microstructure, and chemical distribution of the material's components, characterization at the highest levels of resolution becomes of supreme importance. For these purposes, the high resolution and specificity of electron microscopy, diffraction, and microanalyses currently capable of near atomic synthesis, makes these methods invaluable and prerequisites for successful research and development of advanced ceramics.

The basic principles of these techniques are now well known, and will not be reviewed here.[1–3] The present limitations are illustrated by current research on applications of 'atomic imaging' (HREM), coupled with microdiffraction (notably convergent beam methods) to elucidate structures, e.g. in oxide ceramics. The application of electron energy loss spectroscopy (PEELS) to evaluate ceramics containing light elements not amenable to classical X-ray spectroscopy is also illustrated. The example given here is for fiber composites of BN coated SiC, in SiC matrices. Of course, it should be realized that all the methods of characterization may apply to solving materials problems, but this paper will refer specifically to the HREM and PEELS methods.

2 HREM and Structure Analyses

Since fundamental properties of materials depend on their crystal structures, and defects, and since novel properties, particularly electronic, are now being achieved through novel processing routes, e.g. to obtain nanostructures, thin films, multilayers, etc., crystal structure analyses of materials having small dimensions becomes particularly important. It is in these situations that HREM may become the method of choice, in spite of several restrictions.

One reason for this is that conventional crystallography by X-ray or neutron diffraction is limited in that they provide averaged information from specimens, and as a result may not resolve individual crystals, and defects. Electron microscopy is specific, and is limited mainly by statistics. As an example of these differences, HREM analyses of SiAlON compounds showed the presence of polytypoids[4] in which the structure is determined by the cation/anion ratio as summarized in Table 1. At a ratio of 16/17, X-ray data showed the presence of the 32H polytypoid, whereas HREM results (Fig. 1)

*Invited plenary lecture at the conference on 'Powder Characterization for Advanced Materials Manufacture', Gijon, Spain 16–20 June 1997.
†To whom correspondence should be addressed at the University of California.

Table 1. Polytypoid structures in SiAlONs generated with different cation:anion [M/N] ratios* (after Ref. 4)

n†	*M/N*	*Polytypoid*	*c (nm)*
4	4/5	8 H	2·304
5	5/6	15 R	4·185
6	6/7	12 H	3·288
7	7/8	21 R	5·712
8	8/9	16 H	4·070
9	9/10	27 R	7·209
11	11/12	33 R	8·646
12	12/13	24 H	Not measured
13	13/14	39 R	10·140
16	16/17	32 H‡	8·282‡
∞	1	2H	0·498

*These are observed in many ceramic systems
†Number of layers
‡This is not a true structure but a composite of 21R and 27R blocks.

clearly show the structure to be repeating blocks of 21R and 27R polytypoids. Thus the 32H is not a fundamental structure. Similar cases exist in other compounds, notably the ceramic superconductors[5] and many other materials.[6] Another important point from such studies of polytypoids is that the image actually provides chemical composition information. Of course this can be verified by CBED and microanalysis.

In general, real space crystallographic analyses should be coupled with microdiffraction, and CBED—a subject ever developing with the work of Steeds and colleagues,[7] and requires expertise in diffraction physics—which points to the continuing need for interdisciplinary cooperation in the field of materials science.

3 Atomic Imaging

As an example of a typical structural problem, consider the case of the well-known mineral/ceramic mullite. This material has excellent high temperature and creep properties, and as a matrix can be toughened by composite processing such as with Zirconia[8] or by fiber strengthening of other matrices, such as $MoSi_2$.[9] Mullite is an aluminumsilicate with composition ranging from approximately $3Al_2O_3{\cdot}2SiO_2$ to $2Al_2O_3{\cdot}SiO_2$, which is normally orthorhombic (space group *pbam*) but can be tetragonal depending on composition and processing route, i.e. the structure is not simply a function of composition. The ratio Al_2O_3:SiO_2 (henceforth designated as M:N) characterizes the chemical composition of mullite in terms of the complete formula $Al_{4+2x}Si_{2-2x}O_{10-x}$, where x designates the number of oxygen atoms missing per unit cell. Clearly, $x = 2\{M:N\} - 1/(2\{M:N\} + 1)$ and $M:N = 1 + x/2/(1-x)$.

The problem of direct elucidation of the unit cell is thus complicated because it is necessary to image cations, anions (oxygen) and anion vacancies. Although this may seem to be a daunting task, some success has been achieved already[10] and hope for better results now stems for the availability of microscopes capable of interpretable resolution to 0·1 nm.

For mullite solid solutions, the lattice parameters vary almost linearly with composition,[11] and of course when $a = b \neq c$ the tetragonal structure is attained, and has been reported.[12,13] Examination of mullite whiskers prepared by synthesis of topaz,[14] showed the tetragonal phase existed at compositions below that predicted from lattice parameter considerations. Whiskers obtained from historical Indian 'Wootz' crucibles* were however orthorhombic. These whiskers differed considerably in size (and history) as shown in Fig. 2. As is known from other systems there is a size dependence on structure. For synthetic whiskers between 100 and 500 nm thick, the tetragonal phase occurred at compositions from M:N = 1·63 to 1·83. The thinner Wootz fibers at 10–30 nm thick, were orthorhombic, and remained so even after annealing in vacuum to reduce the SiO_2 content. These data differ from the predictions of Cameron.[15] At compositions $x = 0{\cdot}25$ to 0·32, the synthetic whiskers would be predicted to be orthorhombic, whereas they are tetragonal. After annealing to enrich in Al_2O_3, tetragonality is predicted whereas in fact the structure is orthorhombic! It can be concluded that that the structure, especially vacancy content, is very dependent on the processing. This emphasizes the need for characterization at each stage of processing or development.

Another factor is that relaxation of structure can occur, as composition changes, for example on

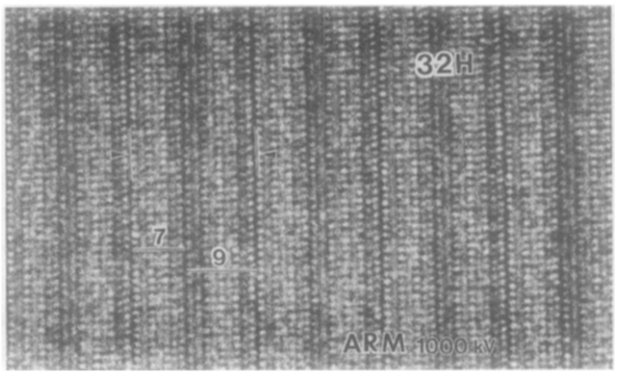

Fig. 1. Lattice image of 21 R and 27 H polytypoid in SiAlON compound with cation:anion ratio of 16:17 (after Ref. 4).

*'Wootz' crucibles were used since the 16th century to carburize irons towards production of 'Damascus' swords. Mullite was formed by the reaction of clay and rice husks (SiO_2).

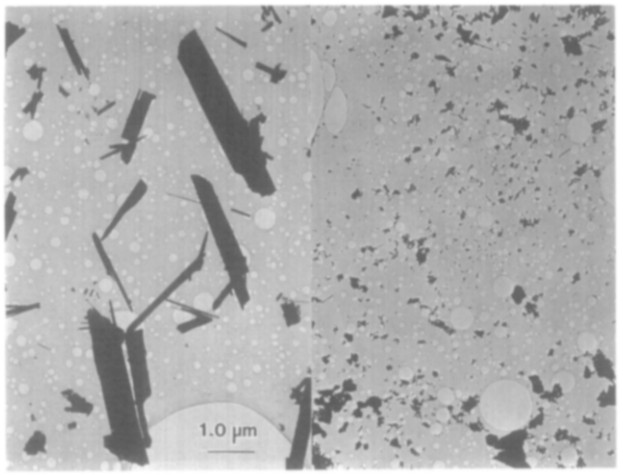

Fig. 2. (a) Fibers of mullite prepared by reaction sintering of topaz (courtesy I. Talmy, N. S. W. C., Silver Spring, MD), and (b) mullite fibers harvested from Indian 'Wootz' crucibles (courtesy T. L. Lowe). Reprinted courtesy *Journal of Material Research.*[14]

annealing whiskers in vacuum to enrich the Al_2O_3 content. Figure 3 is an example for a synthetic whisker 92 nm thick, which has randomly twinned to relieve stresses from volume changes as SiO_2 is removed, but concurrently shows anti-phase boundaries (along 601), signifying oxygen vacancy ordering.[16] This result shows that oxygen vacancies are created during the elimination of the silicon. Thus it is difficult to predict exact structures without knowing in detail all the cationic, anionic and vacancy changes that can occur during processing and subsequent treatments.

What can be expected by improved image resolution? At the current resolution limit of ~1·6A with the Berkeley 800 kV ARM, and by producing remarkably excellent thin films from bulk mullite of composition $x = 0{\cdot}25$ to 0·3, and with detailed calculations for image interpretation, Epicier *et. al.*[10] succeeded in detecting oxygen vacancies in specimens provided the thickness was less than

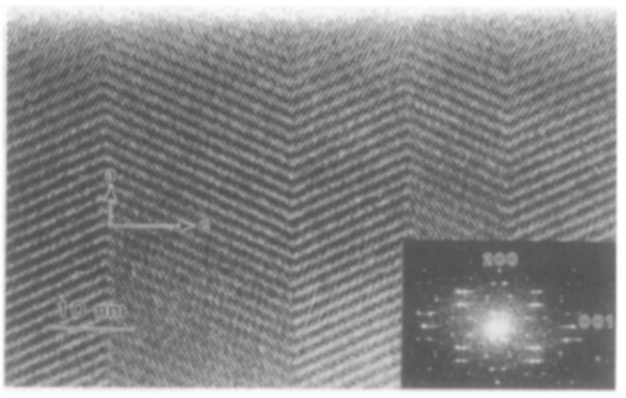

Fig. 3. ARM image in (100) of orthorhombic high alumina synthetic mullite fibers. Notice twinning and periodic (601) anti-phase domain boundaries as expected from oxygen vacancy ordering as SiO_2 content is reduced. Insert shows the selected area laser optical diffraction. Reprinted courtesy *Journal of Material Research.*

2·5 nm. There was no evidence of vacancy (or other) ordering, confirming earlier attempts to atomically image mullite in composites with ZrO_2 and with M:N = 1·7 to 1. The structure seems best described in terms of average orthorhombic unit cells containing disordered vacancies. These detailed studies also show that HREM images are not easily correlated with oxygen vacancy ordering, as also noted by Ylä-Jääski and Nissen.[16] Cationic order is of course seen by superlattice reflections in the diffraction pattern. Long range order is detected also by antiphase boundary contrast (Fig. 3).

Clearly the problem really requires truly atomistic discrimination within the unit cell. Weak phase object calculations of the resolution and thickness requirements to image oxygen positions in the orthorhombic mullite cell are shown in Figs 4 and 5. At 300 kV the thickness limitation is 10 nm even where 0·1 nm resolution is available (as is the case today). Whilst this specimen restriction is severe for bulk ceramics, it falls within size ranges possible in nanostructures. However even at 0·1 nm resolution, Fig. 6 shows that not all oxygen sites are detectable—as also of course for vacancies. It cannot be over-emphasized that the image is still a two-dimensional projection of the three-dimensional object, so many images in different projections must be analyzed. Thus microscopes must have large angle specimen tilting capabilities, as with the 800–1250 kV machines, since tilt capabilities may be restricted by lens design to lower spherical aberration in medium voltage microscopes. This factor must be balanced by radiation damage considerations also, since the probability of atomic displacement increases with accelerating voltage.

It must also be emphasized that coupled with the experimental needs for such resolution, the images can only be interpreted when all the necessary specimen (thickness, tilt, etc.) and instrument (defocus, divergence, etc.) parameters are taken into account by image calculations so as to obtain consistent experimental–theoretical matching.

4 Interfaces—The Final Frontier?

Many of the most important properties of ceramics relate to interfaces—these include grain boundaries, intergranular phases from processing, joining interfaces and so on. Recently, success has been achieved in improving the strength of joints in Si_3N_4 ceramics with Si_3N_4 and with other compatible compounds (e.g. Al_2O_3) by utilizing reaction sintering methods with rare-earth oxides and silica.[17] These silicates have previously been used to densify silicon nitrides,[18] and results in partial

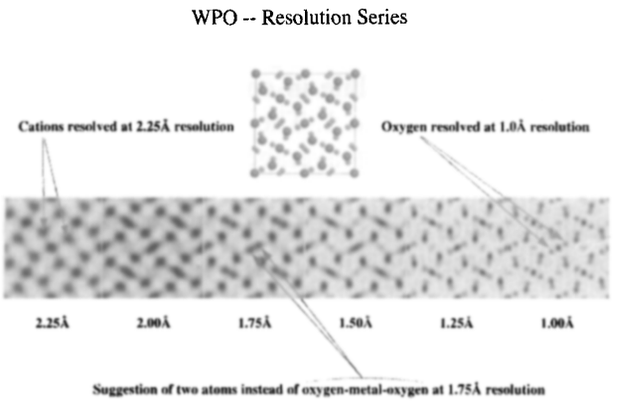

Fig. 4. Weak phase object calculations of images expected from [001] orthorhombic mullite as a function of electron microscopy point-to-point resolution. Notice 0·1 nm is required to locate anions (M. O'Keefe and G. Thomas, research in progress).

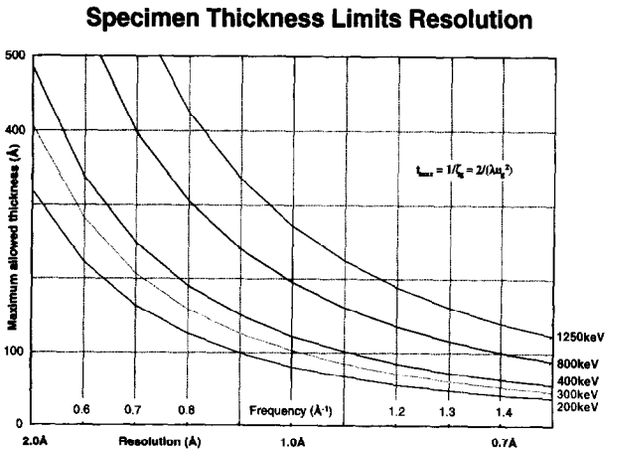

Fig. 5. Kinematical calculations of specimen thickness required to achieve a range of point resolution over a range of accelerating voltages (courtesy M. O'Keefe).

crystallization of the intergranular phase forming $RE_2Si_2O_7$. The high temperature strength,[19] creep[19] and oxidation resistance[20] are also greatly improved by this microstructure.

Nevertheless, in order to completely understand interfaces including heterogeneous ones, e.g. metal–ceramic joints, it is necessary to evaluate the structure, composition and bonding at interfaces. Thus combinations of the most powerful TEM methods—HREM, CBED and PEELS will be required. As discussed above, from a structural viewpoint the resolution needed must be at least 0·1 nm. Figure 6 shows a calculated image at 0·1 nm for a grain boundary in rutile, together with the best resolution currently attainable with the ARM instrument at Berkeley. The experimental image does not identify the atoms at the interface as only cations are resolved. At 0·1 nm resolution, however, the terminating planes at the boundary can be identified. The future for such HREM is clearly exciting for such studies.

In summary, although real-space crystallography of very small crystals is potentially viable, and will

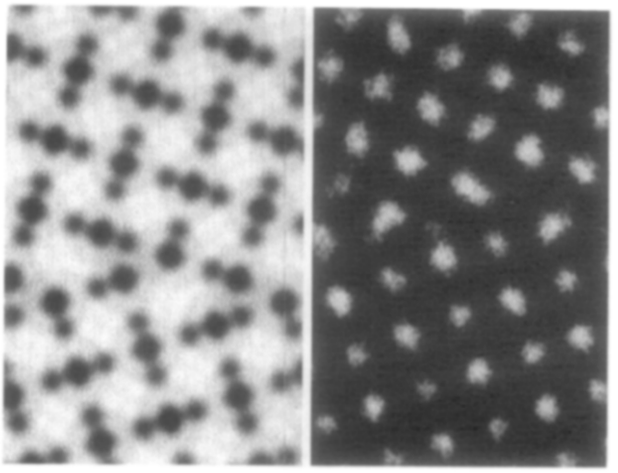

Fig. 6. Calculated image (left) at 0·1 nm resolution compared to experimental image (right) at 0·16 nm resolution for rutile TiO_2. Notice at 0·1 nm, discrimination of oxygen positions is predicted (courtesy M. O'Keefe).

be facilitated at 0·1 nm resolution, and some successes have been recorded, complete analysis is difficult without also involving high resolution diffraction and microanalysis, and the cooperation of experimentalists and theoreticians. With the development of improved instrumentation, such as intense coherent sources by field emission (FEG) and PEELS with energy filtering, discussed below, we can look forward to continued progress in the search for complete characterization of advanced materials.

5 Microanalysis: Peels Applications

For X-ray microchemical elemental analysis, now well established in electron microscopy, the major problem in detection and resolution is the signal to noise ratio of the characteristic X-rays produced by the inelastic scattering of the incident electrons by those in the specimen. Even with high intensity FEG sources, it is difficult to achieve quantitative analysis of light elements ($Z < 6$) due to the small X-ray yield, and care is needed to minimize beam damage. Since low density materials (including ceramics) are of great importance in many structural design considerations for weight savings, light element analysis is particularly challenging.

Fortunately, the capability of parallel electron energy loss spectroscopy (PEELS) (i.e. analysis of those electrons that are inelastically scattered by the sample, including those involved in X-ray emission) has greatly increased our ability to carry out light element analysis. This technique, only quite recently available with FEG sources, also provides elemental distributions by energy filtered imaging. In addition to the facility for light element detection, the fine structure near the absorption edge contains detail pertinent to the bonding, e.g.

scattering due to inter and intra-band excitations. The spatial resolution is mainly limited by the beam diameter, but with a FEG system, it is possible to achieve ~1 nm resolution spatially, with an energy resolution of ~0·1 ev. In principle this allows all elements from H upwards and minimum concentrations of 10^{-4} at% to be detected.[21] However as yet there are no reports of hydrogen detection in materials. Needless to say, since interpretation of data from these methods involves a detailed understanding of the inelastic processes, analysis again requires cooperation with physicists—hence the advantage of national centers with resident expertise.

Here we describe current research on BN coated SiC fibers, in SiC matrices. In these systems, the SiC fibers are coated with a layer of BN to form a weak interface. During fracture of the composite, the crack is deflected by the weak interface causing fiber pull-out, resulting in an increase in toughness.[22] Fig. 7 shows the SEM image of the fractured composite, in which the fibers are clearly pulled-out.

To help analyze these composites, it was necessary to develop background data pertinent to the

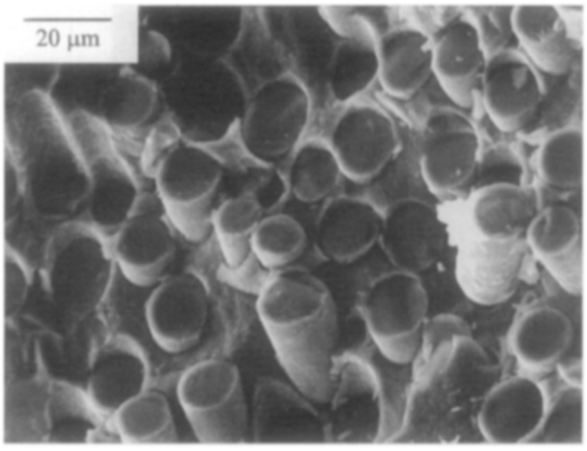

Fig. 7. SEM image of fractured BN-coated SiC fibers in a SiC matrix. Notice pull-out of the fibers.

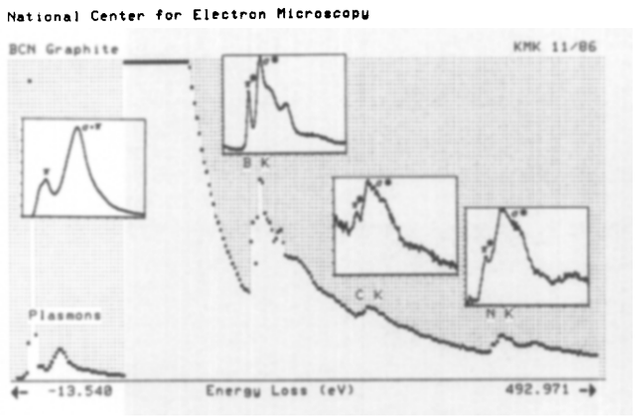

Fig. 8. Electron energy loss and deconvoluted spectra from a CBN 'alloy'. Notice the near edge structure indicating all elements are in the sp2 hybrid bound state, that is graphite (courtesy K. M. Krishnan).

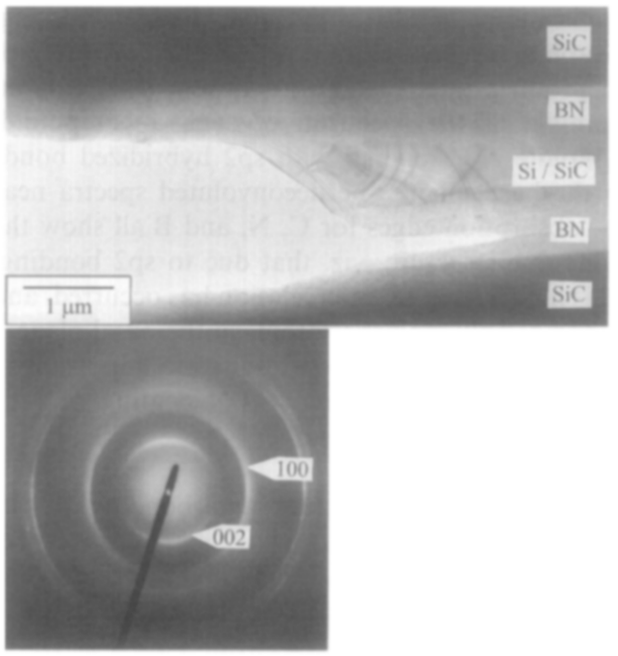

Fig. 9. (a) TEM image of section parallel to fiber axis showing the BN–SiC fiber interface. The matrix consists of SiC precipitates in silicon [Fig. 12 (b)] Electron diffraction pattern from the BN coating showing its basal plane to be parallel to the furface of the fiber.

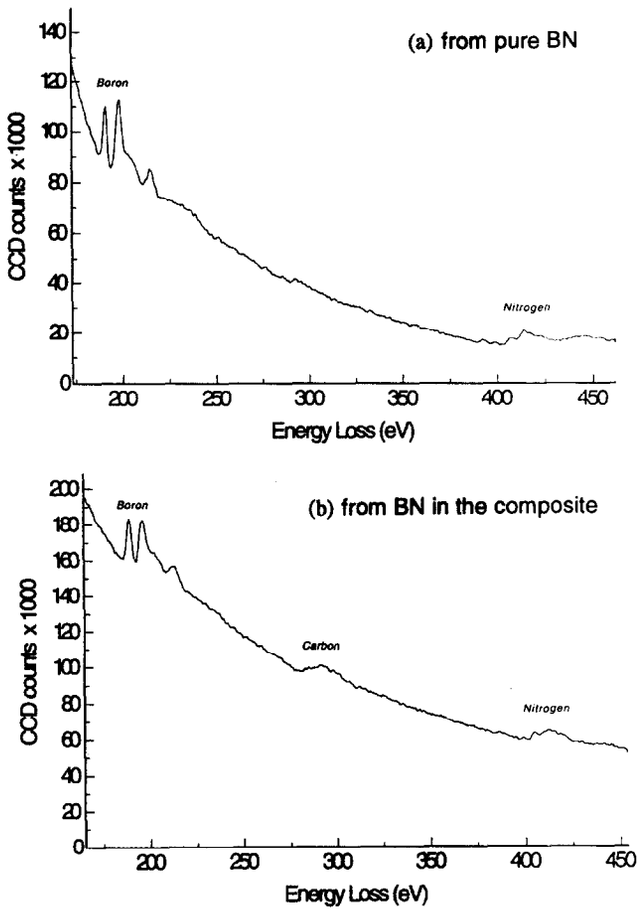

Fig. 10. (a) PEELS spectrum from bulk BN. (b) PEELS spectrum from BN coating from SiC fiber in the composite. Notice appearance of C edge.

application of PEELS, and image filtering. Graphite has been alloyed with B and N to attempt to produce intercalated structures.[23] Fig. 8 is an example of the spectrum of such a compound. Graphite is hexagonal with sp2 hybridized bonds in the basal plane; the deconvoluted spectra near the absorption edges for C, N, and B all show the same fine structure, viz. that due to sp2 bonding. This implies that no intercalation has occurred, and B and N only replace C atoms in the basal plane.

These above mentioned results are important in elucidating the structure of BN coating of SiC. Two main questions arise:

1. What is the structure and bonding of the coating?
2. Has there been any reaction at interfaces during processing of the composites?

Figure 9(a) shows the TEM image obtained by very careful specimen preparation involving dimpling and ion milling. Sections parallel and transverse to the fibers have been examined. Figure 10(a) and (b), are PEELS spectra of bulk BN and from the BN coating respectively. Notice the presence of the C edge in the latter. This means that some reaction has occurred to allow carbon to penetrate the coating. The PEELS spectrum from the fiber coating [Fig. 10(b)] can be compared to that of the synthesized CBN (Fig. 7), and bulk BN [(Fig. 10(a)]. In each case, the fine structure near the absorption edges all indicate the same sp2 bonding and graphitic structures. It should be noted that no oxygen was detected in any of the EELS spectra, from fiber nor coating.

Electron diffraction analyses of BN [Fig. 9(b)] shows the c-axis lattice parameter to be 0·35 nm that is larger than the 0·33 nm in bulk BN. This difference is attributed to either alloying of BN with C,[24] or due to the turbostratic structure of the BN, in which the arrays that form the basal plane are randomly rotated within the plane.[25] The BN diffraction patterns also show texture, with the basal plane of BN being parallel to the surface of

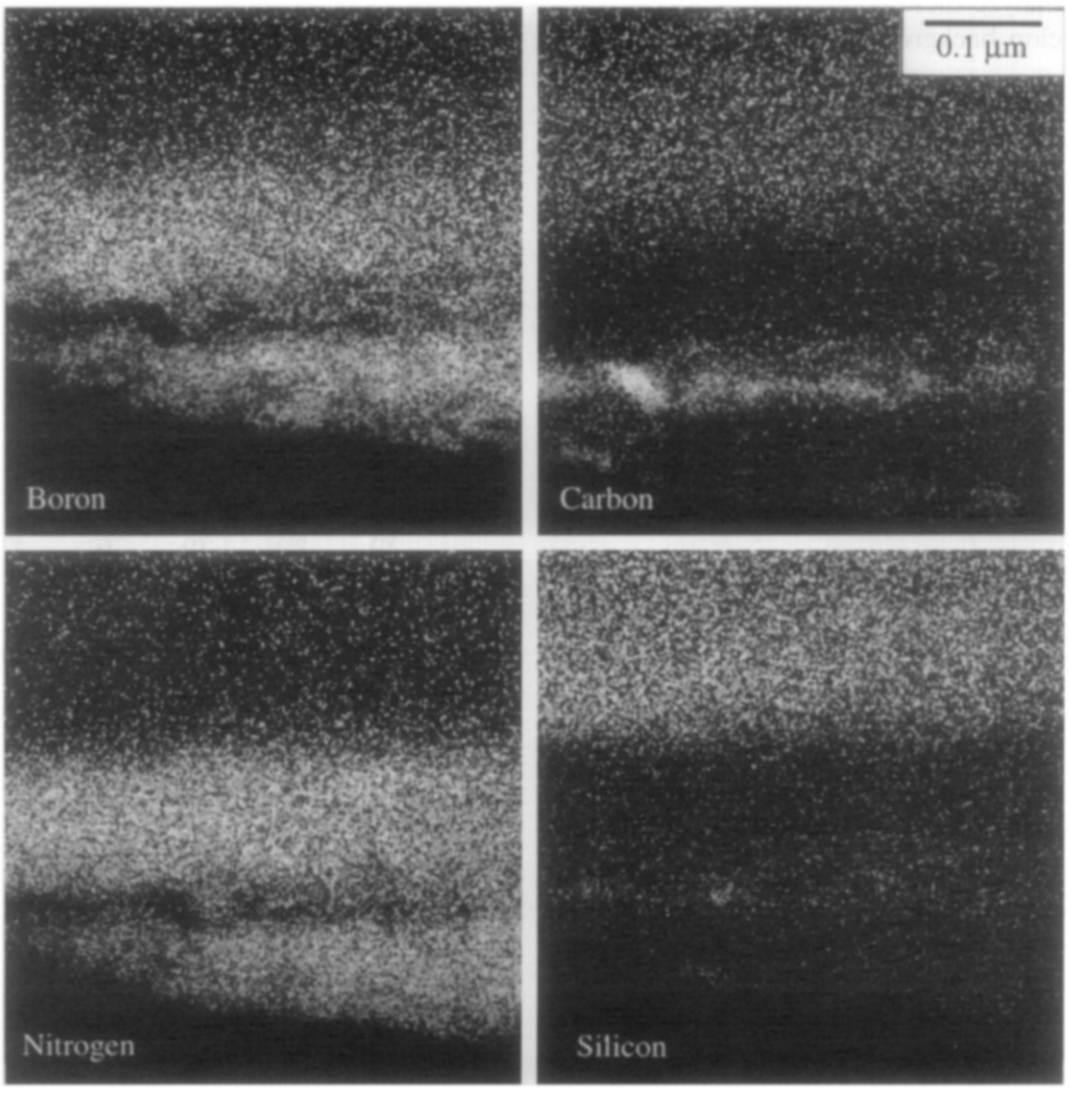

Fig. 11. Energy filtered images corresponding to the elemental distribution of B, C, N and Si. Notice the presence of C and Si within the BN coating.

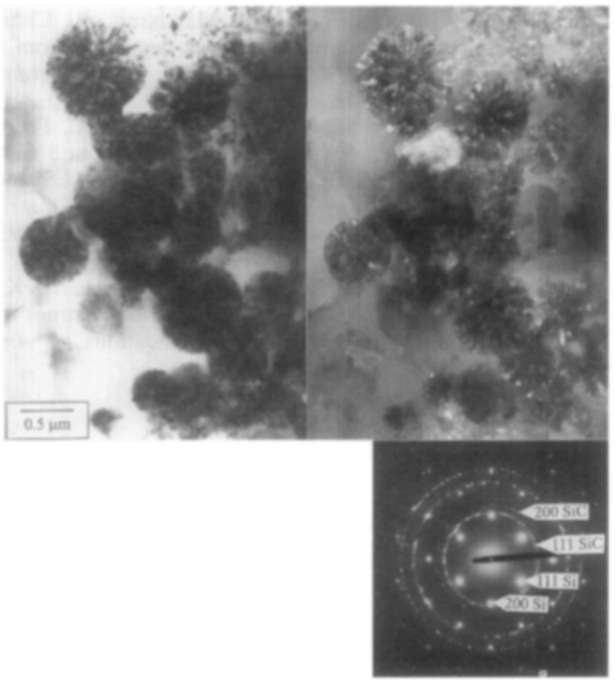

Fig. 12. (a) Bright field and (b) dark field image showing precipitates of of SiC inside a single grain of silicon. (c) Electron diffraction analysis shows the SiC to be the cubic polytypoid.

the fiber. This orientational dependence has been observed and studied in detail by other workers.[26]

The penetration of carbon into the BN coating is verified by the energy filtered imaging of the B, N, C and Si components, shown in Fig. 11 The energy filtered imaging shows strong correlation between regions rich in B and N and regions rich in Si and C. This suggests that these elements are present in their compound form. One possible mechanism for this is by molten Si (used to form the matrix) penetrating the weak SiC/BN interface (in fact, current results show penetration of silicon at these interfaces). Subsequent reaction with carbon, also used to form the SiC matrix, causes formation of SiC. This reaction can be studied in the formation of the matrix. Figure 12 shows cubic-SiC precipitates precipitating inside a large crystal of silicon. This suggests that the carbon dissolves in the Si and precipitates out during the cooling process.

These results indicate the unique capabilities of PEELS analyses for such problems. This analysis, coupled with conventional and high resolution microscopy, can help solve many problems in materials science.

Acknowledgements

This research is supported in part by the Director, Office of Basic Energy Sciences, Division of Materials Sciences of the United States Department of Energy under Contract No. DE-AC-03-76SF 00098. We especially thank the staff at the National Center for Electron Microscopy, particularly M. O'Keefe (atomic imaging) and C. Hetherington and C. Nelson (PEELS imaging) for their help and cooperation. We also thank T. Kameda of Toshiba Corporation for providing the commercial BN–SiC fibers.

References

1. Thomas, G. and Goringe, M. J., Transmission Electron Microscopy of Materials, Tech Books, Fairfax, VA, 1981.
2. Williams, D. B. and Carter, C. B., Transmission Electron Microscopy: A Textbook for Materials Science. Plenum Press, New York, 1996.
3. Thomas, G., Electron microscopy and microanalysis of ceramics. *Journal of the European Ceramic Society*, 1995, **16**(3), 323–338.
4. van Tendeloo, G., Faber, K. T. and Thomas, G., Characterization of AlN ceramics containing long-period polytypoids. *J. Mater. Sci.*, 1983, **18**(2), 525–532.
5. Ramesh, R., Thomas, G., Green, S. and Jiang, C., Polytypoid structure of Pb-modified Bi–Ca–Sr–Cu–O superconductor. *Phys. Rev. B,*, 1988, **38**(10), 7070–7073.
6. Thomas, G. and Ramesh, R., Atomic imaging and microanalysis of ceramics at the NCEM Berkeley California. *Cer. Trans.*, 1990, **5**, 287–314.
7. Steeds, J. W., Quantitative Electron Diffraction. In *IX Conference on Electron Microscopy of Solids*, ed. A. Czyrska-Filamenwoicz *et al.* Fotobit, Krakow, Poland, 1996, 175–182.
8. Schryvers, D., Srikrishna, K., O'Keefe, M. A. and Thomas, G., An electron microscopy study of the atomic structure of a mullite in a reaction-sintered composite. *J. Mater. Res.*, 1988, **3**(6), 1355–61.
9. McFayden, A., $MoSi_2$-Mullite fiber composites. Ph.D. thesis, University of California, Berkeley, CA, 1995.
10. Epicier, T., O'Keefe, M. A. and Thomas, G., Atomic imaging of 3:2 mullite. *Acta Cryst.*, 1990, **A46**(12), 948–962.
11. Okada, K. and Otsuka, N., Synthesis of mullite whiskers by vapor-phase reaction. *J. Mater. Sci. Lett.*, 1989, **8**, 1052–1054.
12. Duvigneaud, P. H., Existence of mullite without silica. *J. Am. Ceram. Soc.*, 1974, **57**(5), 224.
13. Perrotta, A. J. and Young, J. E., Silica-free phases with mullite-type structures. *J. Am. Ceram. Soc.*, 1974, **57**(9), 405–407.
14. Merk, N. and Thomas, G., Structure and compositional characterization of submicron mullite whiskers. *J. Mater. Res.*, 1991, **6**(4), 825–834.
15. Cameron, W. E., Mullite: a substituted alumina. *Am. Mineral.*, 1977, **62**(7–8), 747–755.
16. Ylä-Jääski, J. and Nissen, H.-U., Investigation of superstructures in mullite by high resolution electron microscopy and electron diffraction. *Phys. Chem. Miner.*, 1983, **10**(2), 47–54.
17. Gopal, M., De Jonghe, L. C. and Thomas, G., Silicon nitride joining using rare-earth reaction sintering. *Scripta Mater.*, 1997, **36**(4), 455–460.
18. Cinibulk, M. K., Thomas, G. and Johnson, S. M., Fabrication and secondary-phase crystallization of rare-earth disilicate silicon nitride ceramics. *J. Am. Ceram. Soc.*, 1992, **75**(8), 2037–2043.
19. Cinibulk, M. K., Thomas, G. and Johnson, S. M., Strength and creep behavior of rare-earth disilicate–silicon nitride ceramics. *J. Am. Ceram. Soc.*, 1992, **75**(8), 2050–2055.
20. Cinibulk, M. K., Thomas, G. and Johnson, S. M., Oxidation behavior of rare-earth disilicate–silicon nitride ceramics. *J. Am. Ceram. Soc.*, 1992, **75**(8), 2044–2049.

21. Krivanek, O. L., Kundmann, M. K. and Bourrat, X., Elemental mapping by energy-filtered electron microscopy. In *Determining Nanoscale Physical Properties of Materials by Microscopy and Spectroscopy*, ed. M. Sarikaya, H. K. Wicramasinghe and M. Isaacson. *Mater. Res. Soc. Symp. Proc.*, **332**, 1994, 341–350.
22. Kim, J.-K. and Mai, Y.-W., High strength, high fracture toughness fiber composites with interface control—a review. *Compos. Sci. Technol.*, 1991, **41**(4), 333–378.
23. Kouvatakis, J., Sasaki, T., Shen, C., Hagiwara, R., Lerner, M., Krishnan, K. M. and Bartlett, N., Novel aspects of graphite intercalation by flourine and fluorides and new B/C, C/N, and B/C/N materials based on the graphite network. *Synth. Met.*, 1989, **34**, 1–7.
24. Saugnac, F., Teyssandier, F. and Marchand, A., Characterization of C–B–N solid solutions deposited from a gaseous phase between 900° and 1050°C. *J. Am. Ceram. Soc.*, 1992, **75**(1), 161–169.
25. Dugne, O., Prouhet, S., Guette, A., Naslain, R., Fourmeaus, F., Khin, Y., Sevely, J., Rocher, J. R. and Cotteret, J., Interface characterization by TEM, AES and SIMS in tough SiC (ex-PCS) fiber–SiC (CVI) matrix composites with a BN interphase. *J. Mater. Sci.*, 1993, **28**(13), 3409–3422.
26. Borek, T. T., Qiu, X., Rayfuse, L. M., Datye, A. K., Paine, R. T. and Allard, L. F., Boron nitride coatings on oxide substrates: role of surface modifications. *J. Am. Ceram. Soc.*, 1991, **74**(10), 2587–91.